

Supporting Information:

Accurately predicting the thermal conductivity of boron arsenide due to phonon

anharmonic renormalization:

A critical revisit

Yongjun Wu¹, Yan Zhang¹, Zhen Tong^{1*}

¹School of Advanced Energy, Sun Yat-Sen University, Shenzhen 518107, China

Density Functional Theory Calculations

All *ab initio* calculations are carried out using projector-augmented-wave (PAW) ¹ method with the Perdew-Burke-Ernzerhof exchange and correlation (XC) functional ² as implemented in Vienna Ab initio Simulation Package (VASP) ³. The B $2s^22p^1$ and As $4s^24p^3$ shells are treated as valence states. Kinetic energy cutoff value of 520 eV was used for the wave functions. The force and energy convergence thresholds of 10^{-4} eV/Å and 10^{-10} eV, respectively, were used for both structural relaxation and self-consistent density functional theory (DFT) calculations. The Brillouin zone was sampled with a Monkhorst–Pack mesh of $5 \times 5 \times 5$ for the structure relaxation of BAs with a primitive cell containing 2 atoms. The relaxed lattice constants are $a=4.82$ Å and $\alpha=90.00^\circ$, which is within 1.00 % of the experimental values ($a=4.78$ Å⁴).

Off-diagonal contributions to κ_L

Based on the Wigner transport theory ⁵, the off-diagonal ($s \neq s'$) terms of the Wigner heat-flux operator ⁶ give rise to

$$\kappa_c^{\alpha\beta} = \frac{\hbar^2}{kBT^2VN_q} \sum_q \sum_{s \neq s'} \frac{\omega_q^s + \omega_q^{s'}}{2} v_{q,\alpha}^{s,s'} v_{q,\beta}^{s,s'} \times \frac{\omega_q^s n_q^s (n_q^s + 1) + \omega_q^{s'} n_q^{s'} (n_q^{s'} + 1)}{4(\omega_q^s - \omega_q^{s'})^2 + (\Gamma_q^s + \Gamma_q^{s'})^2} \times (\Gamma_q^s + \Gamma_q^{s'}) \#(S1)$$

In this expression, Γ_q^s ($\tau_q^s = 1/\Gamma_q^s$) is the scattering rate of a phonon mode which includes isotope-phonon, three-phonon (3ph) and four-phonon (4ph) scattering processes. The velocity operator

$v_{q,\alpha}^{s,s'}$ is written as $v_{q,\alpha}^{s,s'} = \sum_{\alpha,\alpha'} e_{q,\alpha}^s \nabla_q^\beta \sqrt{D_q^{\alpha,\alpha'}} e_{q,\alpha'}^{s'}$, in which the $e_{q,\alpha}^s$ is the phonon eigenvectors and \mathbf{D} is the dynamical matrix.

Harmonic and Anharmonic Force Constants

Ground Force Constants Calculations: The ground interatomic force constants (G-IFCs) are calculated at 0 K. The second-order G-IFCs^{2nd} have been computed on a $5 \times 5 \times 5$ supercell with $1 \times 1 \times 1$ \mathbf{k} -points using density functional perturbation theory (DFPT) and accounting for the non-analytic term correction due to the dielectric tensor and Born effective charges, which are then extracted using Phonopy⁷. The third-order G-IFCs^{3rd} have been computed on a $4 \times 4 \times 4$ supercell with Gamma \mathbf{k} -points in which the diameter cutoff distance is limited to 0.8 nm, using finite-displacement approach as implemented in the THIRDORDER.PY script packaged in ShengBTE⁸. The fourth-order G-IFCs^{4th} have been computed on a $4 \times 4 \times 4$ supercell with Gamma \mathbf{k} -points in which the diameter cutoff distance is limited to 0.5 nm, using finite-displacement approach with our in-house code⁹⁻¹¹. The shorter cutoff distance for the G-IFCs^{4th} stems from the earlier observation¹² that high-order IFCs are often more spatially localized, which has been further confirmed with previous works^{10,11,13}. The particle-like component of the thermal conductivity ($\kappa_p^{\alpha\beta}$) formula in Eq. (1) of the main text has been computed using ShengBTE for 3ph⁸ and its extension for 3+4ph¹⁴. The coherence thermal conductivity ($\kappa_c^{\alpha\beta}$) formula in Eq. (S1) of the supporting information has been implemented in the Phono3py package¹⁵ by Simoncelli *et al.*¹⁶. We here developed an in-house extension of Phono3py to involve the 4ph scattering in computing the wave-like contribution. The thermal conductivity ($\kappa_p^{\alpha\beta}$ and $\kappa_c^{\alpha\beta}$) based on G-IFCs has been computed based on a mesh $16 \times 16 \times 16$.

Temperature-dependent Force Constants Calculations: The temperature-dependent interatomic force constants (T -IFCs) which are extracted from the *ab initio* molecular dynamics (AIMD) simulations as implemented in the TDEP package¹⁷. The Born-Oppenheimer molecular dynamics with the PAW¹ method as implemented in VASP³ on a $4 \times 4 \times 4$ supercell containing 128 atoms. The kinetic energy cutoff, the force, and the energy convergence thresholds are set to be 520 eV, 10^{-4} eV/Å and 10^{-10} eV, respectively. For the Brillouin zone integration, we use the Γ -point and

ran the simulations on a grid of temperatures and volumes in the canonical ensemble. Temperature was controlled using a Langevin Thermostat¹⁸. The simulations ran for about 40 ps with a time step of 2 fs. When fitting the IFCs, the cutoffs were set to be 6.0, 5.0, and 3.5 Å for the T -IFCs^{2nd}, T -IFCs^{3rd}, and T -IFCs^{4th}, respectively, after the convergence tests (see Fig. S1). The scalebroad parameter was set to be 0.1, and the results of the convergence tests were shown in Fig. S2. The thermal conductivity ($\kappa_p^{\alpha\beta}$ and $\kappa_c^{\alpha\beta}$) based on the T -IFCs (temperature-dependent phonon frequency and anharmonicity) has been computed based on a mesh $26 \times 26 \times 26$, and specifically, a mesh $18 \times 18 \times 18$ for 3ph and mesh $6 \times 6 \times 6$ for 4ph scattering rates as implemented in TDEP¹⁷ have been used based on the convergence test of κ_L , only including 3rd order anharmonicity, as a function of different \mathbf{q} points along each axis as shown in Fig. S3.

Supplemental Figures

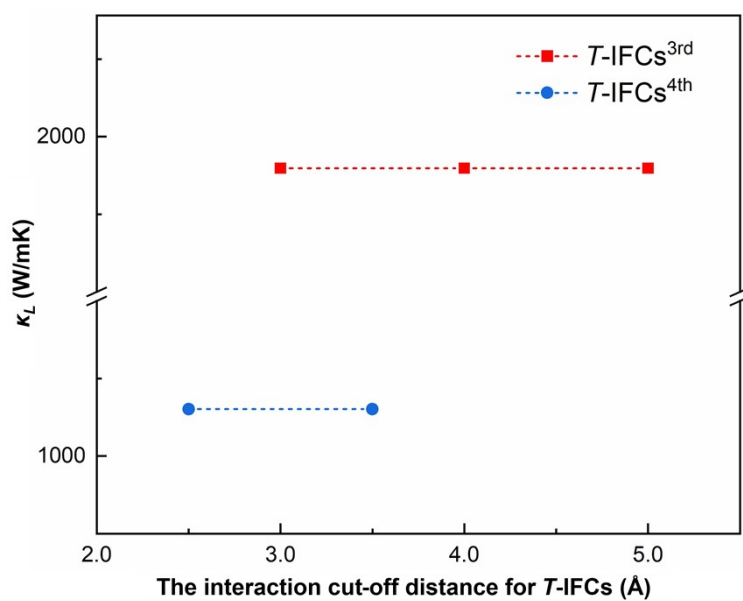


Fig. S1 Calculated κ_L using $T\text{-IFCs}$ with different interaction cut-off distance at 300 K. The red one only includes $T\text{-IFCs}^{3\text{rd}}$ and the blue one includes both $T\text{-IFCs}^{3\text{rd}}$ and $T\text{-IFCs}^{4\text{th}}$.

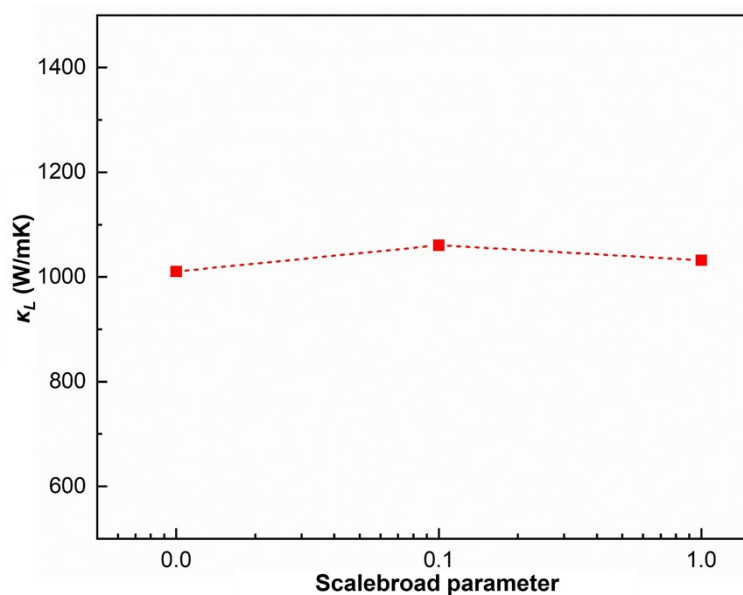


Fig. S2 Calculated κ_L using $T\text{-IFCs}$ with different scalebroad parameter at 300 K.

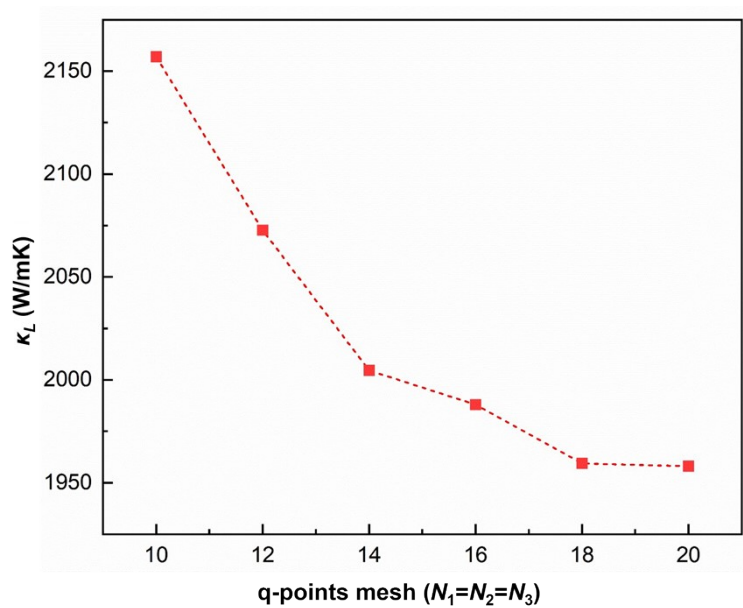


Fig. S3 Calculated lattice thermal conductivity (κ_L) using T -IFCs, only including 3rd order anharmonicity, as a function of different q points along each axis at 300 K.

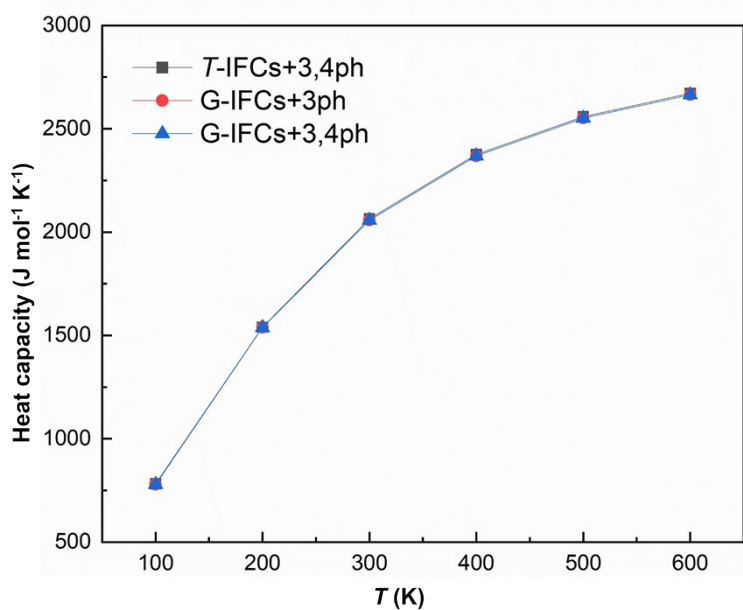


Fig. S4 Comparison of 3ph heat capacity calculated with G-IFCs (red) and 3+4ph heat capacity calculated with G-IFCs (blue) and T -IFCS (black) at $T=100$ K-600 K, respectively.

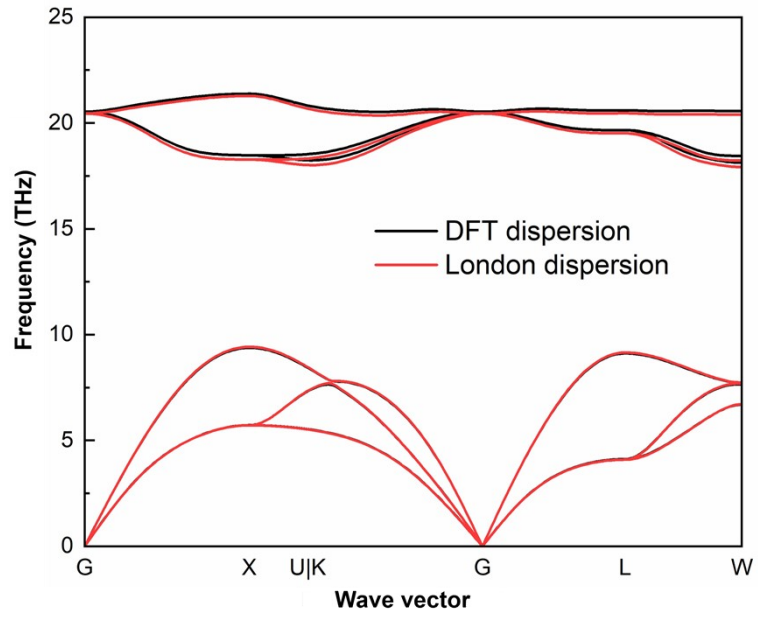


Fig. S5 Comparison of phonon dispersion relations with and without considering London dispersion in natBAs .

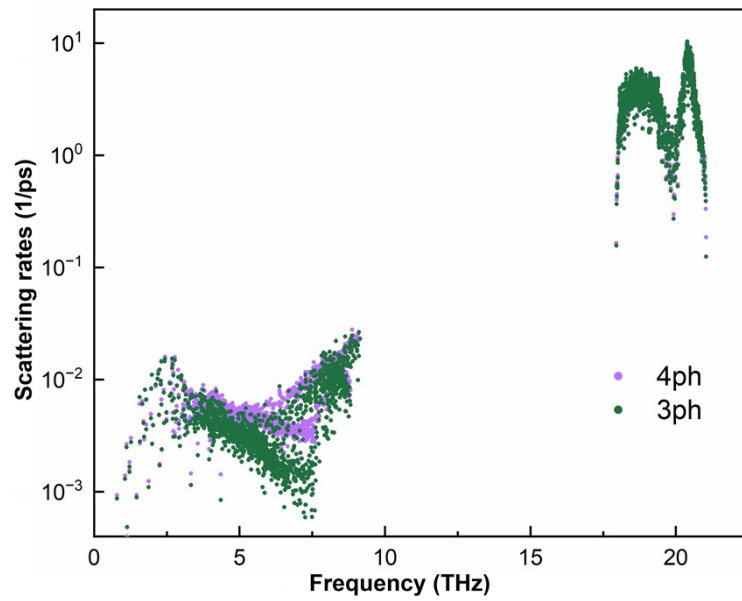


Fig. S6 The 3ph and 4ph scattering rates at 300 K for $T\text{-IFCs}$.

References

- 1 G. Kresse and D. Joubert, From ultrasoft pseudopotentials to the projector augmented-wave method, *Phys. Rev. B*, 1999, **59**, 1758–1775.
- 2 J. P. Perdew, K. Burke and M. Ernzerhof, Generalized Gradient Approximation Made Simple, *Phys. Rev. Lett.*, 1996, **77**, 3865–3868.
- 3 G. Kresse and J. Hafner, *Ab initio* molecular dynamics for liquid metals, *Phys. Rev. B*, 1993, **47**, 558–561.
- 4 J. A. Perri, S. La Placa and B. Post, New group III-group V compounds: BP and BAs, *Acta Crystallogr.*, 1958, **11**, 310–310.
- 5 R. E. Peierls and L. D. Roberts, *Quantum Theory of Solids*, *Phys. Today*, 1956, **9**, 29–29.
- 6 M. Simoncelli, N. Marzari and F. Mauri, Wigner Formulation of Thermal Transport in Solids, *Phys. Rev. X*, 2022, **12**, 041011.
- 7 A. Togo and I. Tanaka, First principles phonon calculations in materials science, *Scr. Mater.*, 2015, **108**, 1–5.
- 8 W. Li, J. Carrete, N. A. Katcho and N. Mingo, ShengBTE: A solver of the Boltzmann transport equation for phonons, *Comput. Phys. Commun.*, 2014, **185**, 1747–1758.
- 9 Z. Tong, X. Yang, T. Feng, H. Bao and X. Ruan, First-principles predictions of temperature-dependent infrared dielectric function of polar materials by including four-phonon scattering and phonon frequency shift, *Phys. Rev. B*, 2020, **101**, 125416.
- 10 Z. Tong, T. Dumitrică and T. Frauenheim, Ultralow Thermal Conductivity in Two-Dimensional MoO₃, *Nano Lett.*, 2021, **21**, 4351–4356.
- 11 Z. Tong, A. Pecchia, C. Yam, H. Bao, T. Dumitrică and T. Frauenheim, Significant Increase of Electron Thermal Conductivity in Dirac Semimetal Beryllonitrene by Doping Beyond Van Hove Singularity, *Adv. Funct. Mater.*, 2022, **32**, 2111556.
- 12 F. Zhou, W. Nielson, Y. Xia and V. Ozoliņš, Lattice Anharmonicity and Thermal Conductivity from Compressive Sensing of First-Principles Calculations, *Phys. Rev. Lett.*, 2014, **113**, 185501.
- 13 Y. Xia, K. Pal, J. He, V. Ozoliņš and C. Wolverton, Particlelike Phonon Propagation Dominates Ultralow Lattice Thermal Conductivity in Crystalline Tl₃VSe₄, *Phys. Rev. Lett.*, 2020, **124**,

065901.

- 14 Z. Han, X. Yang, W. Li, T. Feng and X. Ruan, FourPhonon: An extension module to ShengBTE for computing four-phonon scattering rates and thermal conductivity, *Comput. Phys. Commun.*, 2022, **270**, 108179.
- 15 A. Togo, L. Chaput and I. Tanaka, Distributions of phonon lifetimes in Brillouin zones, *Phys. Rev. B*, 2015, **91**, 094306.
- 16 M. Simoncelli, N. Marzari and F. Mauri, Unified theory of thermal transport in crystals and glasses, *Nat. Phys.*, 2019, **15**, 809–813.
- 17 O. Hellman and I. A. Abrikosov, Temperature-dependent effective third-order interatomic force constants from first principles, *Phys. Rev. B*, 2013, **88**, 144301.
- 18 W. G. Hoover, A. J. C. Ladd and B. Moran, High-Strain-Rate Plastic Flow Studied via Nonequilibrium Molecular Dynamics, *Phys. Rev. Lett.*, 1982, **48**, 1818–1820.